# Ultra-High-Definition Image Deblurring via Multi-scale Cubic-Mixer

**Xingchi Chen**[1] **Xiuyi Jia**[2] **Zhuoran Zheng**[*1]

[1]School of Cyber Science and Technology, Shenzhen Campus, Sun Yat-sen University
[2]School of Computer Science and Engineering, Nanjing University of Science and Technology

arXiv:2206.03678v2 [cs.CV] 15 Jan 2025

## Abstract

Currently, transformer-based algorithms are making a splash in the domain of image deblurring. Their achievement depends on the self-attention mechanism with CNN stem to model long range dependencies between tokens. Unfortunately, this ear-pleasing pipeline introduces high computational complexity and makes it difficult to run an ultra-high-definition image on a single GPU in real time. To trade-off accuracy and efficiency, the input degraded image is computed cyclically over three dimensional ($C$, $W$, and $H$) signals without a self-attention mechanism. We term this deep network as Multi-scale Cubic-Mixer, which is acted on both the real and imaginary components after fast Fourier transform to estimate the Fourier coefficients and thus obtain a deblurred image. Furthermore, we combine the multi-scale cubic-mixer with a slicing strategy to generate high-quality results at a much lower computational cost. Experimental results demonstrate that the proposed algorithm performs favorably against the state-of-the-art deblurring approaches on the several benchmarks and a new ultra-high-definition dataset in terms of accuracy and speed. The URL address for the code is at `https://github.com/zzr-idam/deblur`.

## 1 INTRODUCTION

Blur is ubiquitous in photography, which degrades the quality of human perception and causes serious disturbances to subsequent computer vision analysis. To address the problem, traditional methods [Chen et al., 2019, Dong et al., 2011, Krishnan et al., 2011, Li et al., 2018, Perrone and Favaro, 2014, Sun et al., 2013, Xu et al., 2013] use statistical constraints for image deblurring. However, most of these methods cannot generalize to dynamic scenes by using handcrafted priors.

Recently, deep learning-based methods have been proposed to solve image deblurring. Numerous networks and functional units for image deblurring have been developed, including vanilla convoluted pipeline [Gong et al., 2017, Kaufman and Fattal, 2020], multi-scale networks [Nah et al., 2017, Zamir et al., 2021, Zhang et al., 2019a], residual learning [Chen et al., 2022, Suin et al., 2020], recurrent neural network [Tao et al., 2018, Zhang et al., 2018], attention mechanisms [Chen et al., 2021b, Liang et al., 2021, Tu et al., 2022, Wang et al., 2021b, Wu et al., 2020, Zamir et al., 2022], and GAN-based approaches [Kupyn et al., 2018, 2019, Sui et al., 2021]. Although these approaches achieve state-of-the-art results, these networks usually involve many stacked convolutional kernels or deeply aligned self-attention units to capture the global information of heterogeneous blurs in the spatial domain and consume massive computing resources.

Another research line [Chakrabarti, 2016, Delbracio and Sapiro, 2015b,a, Qin et al., 2021, Xintian et al., 2021] tries to remove blurs based on frequency domain information. These methods obtain Fourier coefficients by fast Fourier transform (FFT) to generate a sharp image with the deep network. However, there are two limitations to these frequency-based methods. First, these methods still need to use large/numerous convolutional kernels to establish long-range dependence of Fourier coefficients and usually under-performing. Second, these methods usually estimate a coefficient tensor acting on the Fourier coefficients to obtain a clear image in the frequency domain, thereby ignoring the real/imaginary parts of the Fourier coefficients in their respective roles. DeepRFT [Xintian et al., 2021] improves upon traditional methods by incorporating a frequency selection mechanism within a transformer-based framework. In contrast, our Multi-scale Cubic-Mixer directly processes the real and imaginary components of Fourier-transformed images using an MLP-based architecture. Furthermore, our slicing scheme optimizes the han-

*The manuscript is under review* (UAI 2025).

dling of ultra-high-definition (UHD) images, enabling real-time processing on a single GPU—an aspect not explicitly addressed by DeepRFT.

We analyze the difference of the real and imaginary components obtained by FFT between the sharp and blurred images, and find that blurs of an image (i.e., an offset of the image pixels) is closely related to the phase change on the frequency domain. We show that combining both the real and imaginary components is necessary for effective image deblurring, especially the change in the real part is more significant. In addition, similar to our view, Wave-MLP [Tang et al., 2022] also provides theoretical support for our research that the real and imaginary parts of the Fourier coefficients undergo mixed splashing to obtain accurate results in the frequency domain space of the image.

To mine frequency domain information with high accuracy, we propose a novel network, named multi-scale cubic-mixer, to capture the long-range dependencies and local characteristics in the frequency domain while keeping all the frequency domain information. Specifically, the proposed multi-scale cubic-mixer performs on the real and imaginary components of the frequency domain in multiple scales to generate several feature maps (three pairs of real-imaginary feature maps). Then, these feature maps are transformed into three new complex tensors by Fourier inverse transform, which are then fused to yield a clear image. Note that the basic cell of our algorithm engulfs the complete input information without a CNN stem, and then acts the input information on *MLPs* at three dimensions ($C$, $H$, and $W$).

Since many mobile device manufacturers have released new ultra-high-definition (UHD) enabled devices (such as smartphones and tablets), the corresponding methods of enhancing UHD have become extremely important. In response, slicing scheme combined with the multi-scale cubic-mixer learning is proposed to deblur arbitrary resolution images. The scheme works on the three color channels of the arbitrary resolution image and enhances the chromaticity and texture details of the arbitrary resolution image by learning a basket of affine transform coefficients. Our method takes less than 25 ms to process a 4K resolution ($3840 \times 2160$) image on a single Titan RTX GPU shader with 24G RAM, which is highly efficient for deployment in practical applications. At the end of this paper, we discuss the limitations, future works, applications and social implications of the model.

The contributions of this paper are summarized as following:

- We propose a multi-scale cubic-mixer with wave-frequency processing framework to estimate the Fourier coefficients of the sharp image from the blurry input by learning MLP in three dimensions. Cubic-mixer can focus on long-range information of the image to provide a wide range of receptive fields, while the fusion module can capture the local structure.
- We propose a slicing scheme to use the spatial variation and color information between the clear and blurred images to enhance a UHD sharp image since MLP-based approaches cannot directly deal with 4K resolution images.
- Experimental results on several synthetic datasets and real-world images demonstrate the proposed algorithm performs favorably against the state-of-the-art image deblurring methods. Our method can run a 4K resolution image at 40 fps.

## 2 PROPOSED METHOD

### 2.1 WAVE-FREQUENCY PROCESSING

Currently, Wave-MLP [Tang et al., 2022] has made a big splash for high-level image processing task. This is thanks to the fact that the real and imaginary parts of the Fourier coefficients as orthogonal signals are fused and splashed into the MLPs. In other words, the real and imaginary parts of the Fourier coefficients are handled independently in the deep MLP network. So far, we have to ask the question: *Is it possible to split the real and imaginary parts of the Fourier coefficients as wave and particle signals to be processed independently for the deblurring task?* The answer is yes.

In this study, we design a framework of **W**ave-**F**requency **P**rocessing (WFP) to filter the real and imaginary components of the blurry input. We begin our analysis using the example shown in Figure 2. As shown, a blurry image and its real and imaginary parts after FFT are shown in Figure 2(a)-(c), respectively. With the image clears, both the real and imaginary components are changed from the high-frequency to a low-frequency domain as shown in Figure 2 (e) and (f). The main reason is that the real and imaginary components of the Fourier coefficients correspond to the phase change $\varphi$ of the image in the frequency domain (i.e., the displacement of the pixels in the spatial domain),

$$\varphi = \arctan(\mathcal{F}_i(B)/\mathcal{F}_r(B)), \tag{1}$$

where $\mathcal{F}_r(B)$ and $\mathcal{F}_i(B)$ denote the real component and imaginary component extracted by FFT of the blurry input $B$, respectively, and arctangent (arctan) refers to the inverse tangent function. The phase spectrum of the image retains information about the edges and the overall structure of the image [Ghiglia and Pritt, 1998]. Based on the observation from Figure 2, it is confirmed that our motivation is supported by physical meaning. Furthermore, it is known from quantum theory that the entropy increases during the transmission of orthogonal signals in the form of probability clouds, which requires a deep network to observe it. Therefore, we set up two parallel depth subnetworks to run the real and imaginary parts of the Fourier coefficients.

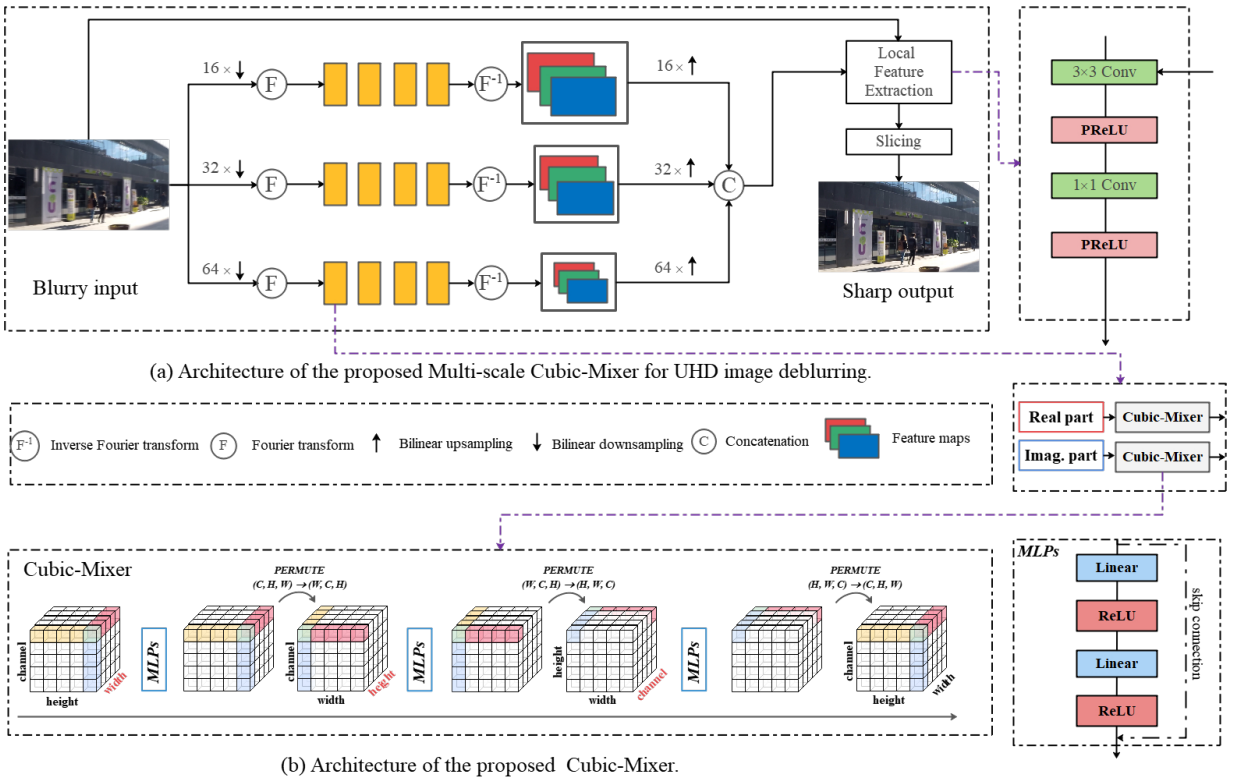



Figure 1: (a) shows the architecture of the proposed single image deblurring network, which consists of three parts. The first part starts with three-path low resolution (LR) feature maps prediction stream (multi-scale cubic-mixer) that learns the frequency domain information to predict a basket of full-resolution feature maps. The second part learns a high quality local feature (attention tensor with 6 channels) by using CNNs with PReLU. The last part generates a full-resolution clear image via slicing scheme. Our proposed algorithm supports UHD image deblurring at 25 ms on a single Titan RTX GPU shader. (b) shows the architecture of the Cubic-Mixer. The basic framework of the model is proposed in modified MLP-Mixer, and we expand one dimension.

We propose the WFP framework for image deblurring, which can be formalized as

$$I = \mathcal{F}^{-1}(\mathcal{C}\{\phi_1(\mathcal{F}_r(B)), \phi_2(\mathcal{F}_i(B))\}), \quad (2)$$

where $\phi_1$ and $\phi_2$ denote the mirror networks that act on the real and imaginary component, respectively; $\mathcal{C}$ indicates the Fourier coefficients combined from the features of the real part $\phi_1$ and the imaginary part $\phi_2$. Finally, the mapped Fourier coefficients is transformed to the sharp image $I$ by performing inverse Fourier transform ($\mathcal{F}^{-1}$). However, we note that if we choose the lightweight deblurring networks [Kupyn et al., 2019, Nah et al., 2017, Suin et al., 2020] as $\phi_1$ and $\phi_2$, we cannot directly handle 4K resolution images in a single GPU shader with 24G RAM by using the WFP framework. Therefore, we propose to reformulate Eq.(2) as:

$$I = \{\mathcal{F}^{-1}(\mathcal{C}\{\phi_1(\mathcal{F}_r(B_\downarrow)), \phi_2(\mathcal{F}_i(B_\downarrow))\})\}\uparrow, \quad (3)$$

where $I$ is obtained by deblurring $B$ in a down-sampled $\downarrow$ resolution first, and then reconstructed by bicubic interpolation $\uparrow$.

## 2.2 PIPELINE

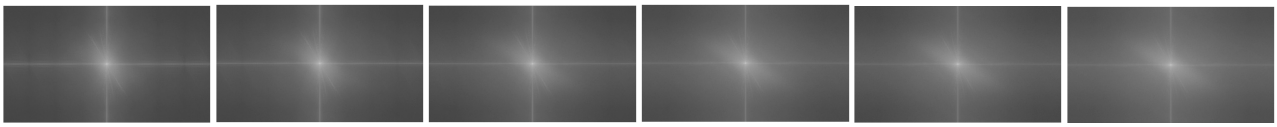
Given a UHD blurry image $B \in \mathbb{R}^{(W \times H \times C)}$, we use the multi-scale cubic-mixer to recover Fourier coefficients for a down-sampled sharp image reconstruction in the frequency domain. Then, we propose a slicing scheme to generate a transform coefficient with a compact structure, which is used to reconstruct the high-definition sharp image from the output of the multi-scale cubic-mixer. Figure 1 illustrates the architecture of the proposed UHD image deblurring network.

**Multi-scale cubic-mixer.** The mainstream of deblurring networks usually under-performing on resource-constrained devices since they over-rely on self-attention scheme to model relationship of the token. To address this problem, we apply a multi-scale cubic-mixer, as shown in Figure 1 (a), to recover sharp images by establishing long-range dependencies on the frequency domain. The cell of multi-scale cubic-mixer is constructed by paralleling two identical cubic-mixer with the WFP framework (Eq.(3)) in the yellow block of Figure 1 (a).



(a) Blurry image (b) Real part of (a) (c) Imag. part of (a) (d) Sharp image (e) Real part of (d) (f) Imag. part of (d)

Figure 2: This figure shows that the change in the real/imaginary part of the Fourier coefficients on a pair of clear/blurred images. Note that the Fourier coefficients are normalized (the pixel range is 0∼10) and executed on images sampled at 64 ×.



(a) Blurry image (b) 1th (c) 2th (d) 3th (e) 4th (f) Sharp image

Figure 3: This figure shows the spectrum of the output of each yellow block in the top path of the network. With the propagation of data through the network, the output spectrum of the trailing yellow block is closer to the spectrum of the clear image. Note that the output of each yellow block is transformed into a complex tensor before being rendered.

The main components of the cubic-mixer are the fully-connected layers based on modified MLP-Mixer. The cubic-mixer achieves the 'mixing' enhancement of element spatial position and channel information in the frequency domain, which can capture long-range of perceptual fields. Compared to MLP-Mixer [Tolstikhin et al., 2021], there are two improvements, i) our model does not conduct the input information in patches, and the native input information is swallowed into the deep network, and; ii) what comes naturally is that we have one more dimensional signal to process than MLP-Mixer, here we establish the long-range dependencies by rolling on three dimensions $C$, $H$, and $W$.

For instance, one path of the proposed network consists of 4× cubic-mixer with WPF framework (the yellow blocks). Every cubic-mixer includes three *MLPs*, and each *MLPs* involves two linear layers as well as the corresponding activation layer. The first *MLPs* mixtures the width-dimension with shared parameters, maps $\mathbb{R}^W \rightarrow \mathbb{R}^W$. The second *MLPs* mixtures the height-dimension with shared parameters, maps $\mathbb{R}^H \rightarrow \mathbb{R}^H$. The last *MLPs* mixtures the channel-dimension with shared parameters, maps $\mathbb{R}^C \rightarrow \mathbb{R}^C$. Specifically, for the input tensor $X \in \mathbb{R}^{(W\times H\times C)}$, the transformation in each mixer layer can be written as follows (the mixer layer index is omitted):

$$F_{i,*,*} = X_{i,*,*} + w_2\sigma\Big(w_1(X)_{i,*,*}\Big), \quad \text{for } i = 1...W \quad (4)$$

$$F_{*,j,*} = F_{*,j,*} + w_4\sigma\Big(w_3(F)_{*,j,*}\Big), \quad \text{for } j = 1...H \quad (5)$$

$$F_{*,*,k} = F_{*,*,k} + w_6\sigma\Big(w_5(F)_{*,*,k}\Big), \quad \text{for } k = 1...C \quad (6)$$

where $w_i$ is the parameter of the $i$th fully connected layer, $\sigma$ is the ReLU function.

Specifically, we downsample the blurry input $B$ to a low-resolution of $B_\downarrow \in \mathbb{R}^{(960\times 540\times C)}$ in the top path, and then feed the Fourier coefficients $\mathcal{F}_r(B_\downarrow)$ into cubic-mixer. The proposed cubic-mixer has three rolls, and each roll consists of *MLPs* as shown in Figure 1(b).

The real part and the imaginary part feed into two cubic-mixer respectively to obtain the real part features and the imaginary part features. Finally, they are combined into a complex number tensor to obtain the feature maps in spatial domain $I$ through $\mathcal{F}^{-1}$. The middle and bottom paths in the network are mirror versions of the top path, where the hidden layer is a fixed value for the input dimension. In addition, we show the Fourier coefficient change in the top path of the network as shown in Figure 3.

**Local feature exaction and slicing enhancement.** Although the multi-scale cubic-mixer has the capability to construct a low-cost global perspective on a blurred image, local rendering can still be bad. To this end, we use several convolutional layers to learn the local features of a blurred image in complementary manner. Specifically, as shown in Figure 1(a), our network splashes out of the three groups of feature maps are upsampled to three high-quality feature maps ($F_t$, $F_m$, and $F_b$), respectively. The raw image $B$, $F_t$, $F_m$, and $F_b$ are concatenated together to obtain a full-resolution tensor $T$ on the channel domain. Next, $T$ passes through the $3 \times 3$ and the $1 \times 1$ convolutional layer and the corresponding activation layer (PReLU), where two items need to be noted. $3 \times 3$ convolutional layer does not change the number of channels, while $1 \times 1$ convolutional layer squeezes the number of channels of $T$ to 6, which prepares the appetizer for the later slicing operation.

Inspired by bilateral learning [Zheng et al., 2021], for UHD images, instead of directly regressing the enhanced image, we can fit a tensor $T$ with the attention characteristics to act on the original image. Specifically, $T$ is regarded as three



(a) $W_{red}$ (b) $W_{green}$ (c) $W_{blue}$ (d) $b_{red}$ (e) $b_{green}$ (f) $b_{blue}$

Figure 4: This figure shows the characteristics of each feature map in the slicing operation, and it is clear that the details acting on the three groups of feature maps in the color channel are complementary to each other.

groups of affine transform operations ($W_{red}$, $b_{red}$; $W_{green}$, $b_{green}$; $W_{blue}$, $b_{blue}$) on the three channels of the original image $B$. We can formalize it as:

$$I_{sharp}(r) = W_{red} \odot B_{red} + b_{red}, \tag{7}$$

$$I_{sharp}(g) = W_{green} \odot B_{green} + b_{green}, \tag{8}$$

$$I_{sharp}(b) = W_{blue} \odot B_{blue} + b_{blue}. \tag{9}$$

As shown in the Figure 4, the three channels of the original image are affine transformed into a sharper spatial domain. These feature maps complement each other's texture details on the color channels. **The polynomial slicing method** is also considered, i.e., given a quadratic ($(W \odot B + b)^2$) to obtain a sharp image. The details are described in the supplementary material.

### 2.3 LOSS FUNCTION

We optimize the weights and biases of the proposed network by minimizing the $L_1$ and perceptual loss [Johnson et al., 2016] on the training set,

$$\mathcal{L} = \frac{1}{N} \sum_{i=1}^{N} \left\| \hat{I}_i - J_i \right\| + \lambda \mathcal{L}_p, \tag{10}$$

where $N$ is the number of training images, $\hat{I}$ is the deblurred result by our model, and $J$ is the corresponding ground truth. The weight $\lambda$ of the loss term $\mathcal{L}_p$ is set to 0.03 in our experiments. We use VGG19 [Simonyan and Zisserman, 2015] as the pre-trained model for the perceptual loss function. We also try to use the total variation and adversarial losses, but we notice that the $L_1$ and $\mathcal{L}_p$ can generate vivid colors and clear texture in the deblurred results.

## 3 EXPERIMENTS

In the section, we evaluate the proposed algorithm on both synthetic datasets and real-world 4K images against the state-of-the-art image deblurring methods in terms of accuracy and visual effect. In addition, we conduct three ablation studies to demonstrate the effectiveness of each module of our method. The implementation code and datasets will be available to the public for further discussion and research. More results can be found in the supplementary material.

### 3.1 DATASET

Although Deng et al. [Deng et al., 2021] build a blurry dataset with 4K resolution, there are less than 100 scenes, for which we expand this dataset. We expand the new 4KRD dataset with two main schemes: frame interpolation and dataset synthesis. The video capturing devices are three mainstream mobile phones (e.g., iPhone 11 Pro Max, Samsung S20 Ultra, and HUAWEI Mate 30 Pro). High frame rates are necessary for the subsequent multi-frame fusion to ensure the fluidity and stability of frames in the synthetic dataset. Due to hardware configuration limitations, we cannot directly capture 4K videos at high-frame-rates with smartphones. Therefore, we use the frame interpolation method [Niklaus et al., 2017] to interpolate the recorded 4K video from 30/60 fps to 480 fps as the scheme in [Nah et al., 2019]. Then we generate blurry frames by averaging a series of successive sharp frames. We synthesized a total of 40 different scene data sets, each scene has 100 images. In addition to our 4K resolution dataset, we also use the public GoPro [Nah et al., 2017], RealBlur-J [Jaesung et al., 2020], and RealBlur-R [Jaesung et al., 2020] datasets to evaluate the effectiveness of our model.

### 3.2 PERFORMANCE COMPARISONS

We compare our algorithm against four state-of-the-art deblurring methods of MPRNet [Zamir et al., 2021], Restormer [Zamir et al., 2022], NaFNet [Chen et al., 2022], MAXIM [Tu et al., 2022].

**Implementation details.** All the experiments are implemented in PyTorch 1.10 and evaluated on a single NVIDIA Titan RTX 3090 GPU with 24GB RAM. The batch size is set to 16 during training. The Adam optimizer is used to train our models with patch size of $1152 \times 648$. The initial learning rate is set to $10^{-4}$. Due to the recent deburring models [Chen et al., 2022, Tu et al., 2022, Zamir et al., 2022, 2021] cannot directly deblur UHD images on a single Tian RTX GPU, we design the splitting-deblurring-stitching (SDS) scheme for the compared deblurring methods on UHD images. The SDS method applies deblurring approaches at the full-resolution image, then stitches these patches (16$\sim$32 patches) to generate a clear 4K image. All the compared methods are fine-tuned on our 4KRD training dataset, we uniformly use SGD optimizer with learning rate

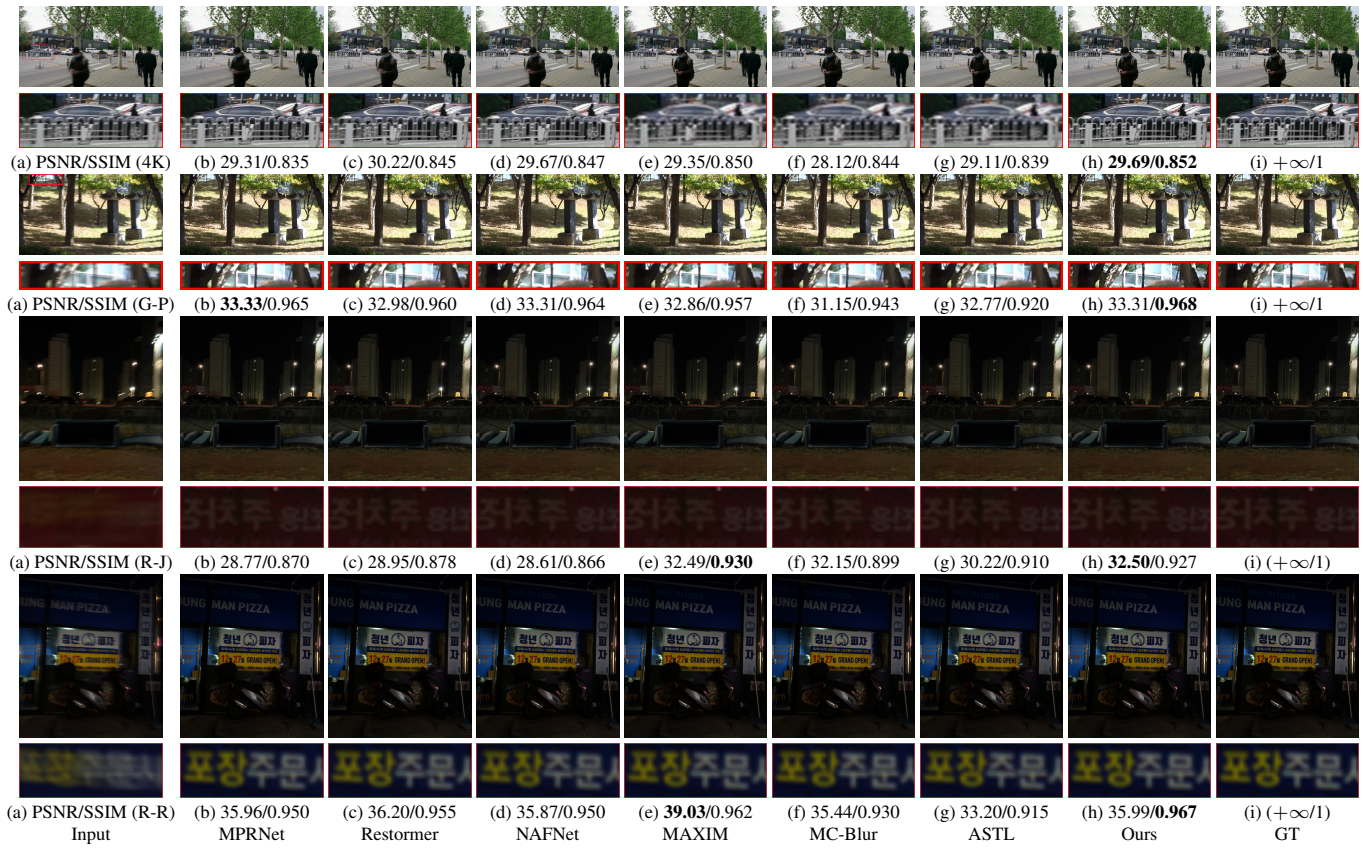



Figure 5: Qualitative evaluations on G-P (GoPro), R-J (RealBlur-R), R-R (RealBlur-J) and 4K (4KRD) datasets. Our proposed multi-scale cubic-mixer generates much clearer details and sharp edges. (Zoom in for best view)

set to 0.001 and epoch set to 16. Note that we do not use any data augmentation methods.

**Quantitative evaluation.** The proposed method is evaluated on four datasets: test data of 4KRD, GoPro, RealBlur-J, and RealBlur-R. Sample results for the proposed method and compared approaches are shown in Figure 5. It can be observed that recent deep models [Chen et al., 2022, Tu et al., 2022, Zamir et al., 2022, 2021] still remain some residual blurs in the results. In contrast, the deblurred results generated by our algorithm are close to the ground truth images in Figure 5(f). Our method achieves the best performance compared to other state-of-the-art methods on the 4K dataset as shown Figure 6. In addition, more detailed quantitative results on the 4KRD, RealBlur-J, RealBlur-R and GoPro datasets are reported in Table 1, which demonstrates the effectiveness of the proposed method.

**Qualitative evaluation.** We also compare our algorithm against other methods on two real-world 4K blurry images, shown in Figure 6. While other state-of-the-art methods produce varying degrees of residual blurs and artifacts, our algorithm yields sharper edges and contain fewer artifacts, shown in Figure 6(f).

### 3.3 ABLATION STUDY

To demonstrate the effectiveness of each module in the proposed network, we perform ablation studies involving the following five experiments. In addition, as shown in Figure 8, we select a low-resolution image for the ablation experiment to demonstrate.

**Effectiveness of real/imaginary part.** To fairly verify the role of real and imaginary parts with the WFP framework, we run the input of double the real part information (named d-real) or double the imaginary part information (named d-imag.) with the WFP on the GoPro dataset. Table 2 demonstrates that the effectiveness of only relying on the information of the real or imaginary parts of the Fourier coefficients to reconstruct the blurred image is discounted.

**Effectiveness of cubic-mixer.** To evaluate the effectiveness of the proposed cubic-mixer, we use the U-Net to replace the proposed cubic-mixer using the WFP framework (named w/o CM). Table 2 demonstrates the effectiveness of the proposed cubic-mixer on the GoPro dataset, which demonstrates that cubic-mixer generates richer textural and color.

**Effectiveness of multi-scale.** We retain only the top path in the network (named w/o MS), and to be fair, we add



(a) Input (b) MPRNet (c) Restormer (d) NaFNet (e) MAXIM (f) MC-Blur (g) ASTL (h) Ours

Figure 6: Deblurred results on real-world 4K resolution images. Our method recovers more image details compared with other state-of-the-art methods.

Table 1: Quantitative evaluations on the 4KRD test data and other datasets in terms of PSNR, SSIM. Although our method does not perform best on publicly available low-resolution datasets (GoPro, RealBlur-R, and RealBlur-J), it has a highly remarkable advantage on 4KRD datasets. **Bolded black** indicates first rank, red and blue indicate second and third rank. Our method is performed 5 $\times$ with cross-validation to obtain an accuracy result.

| Method | GoPro | | RealBlur-R | | RealBlur-J | | 4KRD | |
|---|---|---|---|---|---|---|---|---|
| | PSNR ↑ | SSIM ↑ | PSNR ↑ | SSIM ↑ | PSNR ↑ | SSIM ↑ | PSNR ↑ | SSIM ↑ |
| MPRNet [Zamir et al., 2021] | 32.66 | 0.959 | **39.31** | **0.972** | **31.76** | **0.922** | **28.64** | **0.865** |
| Restormer [Zamir et al., 2022] | **32.92** | **0.961** | 36.19 | 0.957 | 28.96 | 0.879 | 26.88 | 0.830 |
| NaFNet [Chen et al., 2022] | **33.69** | **0.967** | 37.69 | **0.966** | 29.39 | 0.910 | 27.19 | 0.839 |
| MAXIM [Tu et al., 2022] | 32.86 | **0.961** | **39.45** | 0.935 | **36.15** | **0.949** | **30.19** | **0.891** |
| MC-Blur [Yang and Yamac, 2022] | 31.80 | 0.948 | 35.85 | 0.950 | 28.70 | 0.870 | 26.50 | 0.820 |
| ASTL [Zhang et al., 2019b] | 32.25 | 0.936 | 37.80 | 0.964 | 30.25 | 0.910 | 27.80 | 0.845 |
| Ours | **33.79** | **0.962** | **39.66** | **0.969** | **36.75** | **0.953** | **33.89** | **0.916** |

Table 2: Effectiveness of the real/imag. part, cubic-mixer, multi-scale, slicing scheme, and the local feature extraction. Quantitative results demonstrate the effectiveness of each module.

| | d-real | d-imag. | w/o CM | w/o MS | w/o SS | w/o LFE |
|---|---|---|---|---|---|---|
| PSNR | 27.65 $\pm$ **0.11** | 25.87 $\pm$ **0.08** | 31.44 $\pm$ **0.15** | 32.49 $\pm$ **0.12** | 31.98 $\pm$ **0.09** | 33.52 $\pm$ **0.009** |
| SSIM | 0.877 $\pm$ **0.009** | 0.859 $\pm$ **0.010** | 0.939 $\pm$ **0.008** | 0.942 $\pm$ **0.006** | 0.953 $\pm$ **0.007** | 0.960 $\pm$ **0.002** |

some cubic-mixers to the top path to maintain the balance of computational complexity. Note that we can only add 6 cubic-mixers to the top path due to the large resolution of the image. Table 2 demonstrates the effectiveness of the proposed multi-scale on the GoPro dataset, which demonstrates that multi-scale techniques can boost the performance of the model.

**Effectiveness of slicing scheme.** We replace the slicing scheme (named w/o SS) with bilateral grid learning and compare it with our proposed algorithm. Specifically, after local feature extraction we use a downsampling method to generate the biggest bilateral grid ($12 \times 64 \times 16 \times 16$) that can be processed on a single GPU with 24G RAM, and then apply and slice the raw image. Table 2 also demonstrates the effectiveness of the proposed slicing scheme.

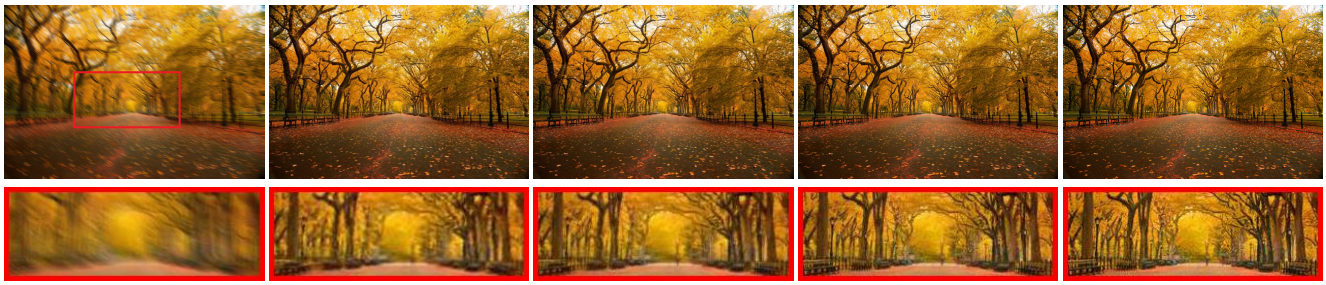
**Effectiveness of local feature extraction.** We use $1 \times 1$ convolution to replace the $3 \times 3$ convolution (named w/o LFE) in the part of local feature extraction. Table 2 demonstrates the effectiveness of the $3 \times 3$ convolution in the local feature extraction.

Furthermore, we combine the comparison methods [Chen et al., 2022, Tu et al., 2022, Zamir et al., 2022, 2021] with the slicing scheme to verify the effectiveness on the 4KRD dataset. As shown in Figure 7, our approach produces sharper edges, fewer artifacts, and better fine detail preservation compared to grid slicing schemes in the restored images.



(a) Input (b) w/o SS (c) Grided Slicing (d) Ours (e) GT

Figure 7: Our method produces sharper edges and restores finer details compared to other approaches.



(a) Input (b) w/o CM (c) w/o SS (d) Ours (e) GT

Figure 8: Our method obtains better visual quality and recovers more image details compared with other ablation experiments. Note that we do not show w/o MS and w/o LFE because the quantitative results are very close and almost visually indistinguishable.

Table 3: Performance on DPDD (defocus blur) and Rain100L (derain) datasets.

| Method | Dataset | PSNR (↑) | SSIM (↑) |
|---|---|---|---|
| IFAN [Lee et al., 2021] | DPDD | 25.37 | 0.789 |
| Restormer [Zamir et al., 2022] | DPDD | 25.98 | 0.811 |
| **Ours** | DPDD | **27.11** | **0.855** |
| MPRNet [Zamir et al., 2021] | Rain100L | 36.40 | 0.965 |
| Restormer [Zamir et al., 2022] | Rain100L | 38.99 | 0.978 |
| **Ours** | Rain100L | **38.82** | **0.977** |

### 3.4 RUN TIME AND POTENTIAL OF THE MODEL

In terms of run time, the proposed multi-scale cubic-mixer model performs favorably against all the comparison deblurring approaches [Chen et al., 2022, Tu et al., 2022, Zamir et al., 2022, 2021]. All the approaches are evaluated on the same machine with an Inter(R) Xeon(R) CPU and an NVIDIA Tian RTX 3090 GPU. Note that the time is only the processing time of the GPU without considering the run time of I/O operations. With the SDS method, it takes 100 ms for MPRNet, 124 ms for Restormer, 98 ms for NaFNet and 279 ms for MAXIM to run a 4K resolution image. These deep models are clearly less efficient than our algorithm.

**Other task.** To assess the generalization ability of our method, we conducted experiments on the DPDD dataset (defocus blur) and Rain100L (derain). These datasets evaluate the robustness of our approach beyond UHD image deblurring. As shown in Table 3, our method outperforms existing approaches in both deraining and defocus blur removal tasks.

**Cubic-Mixer vs. Wave-MLP on ImageNet.** So far, we attempt to use cubic-mixer in an image classification task to verify its effectiveness. We conduct image classification experiments on ImageNet, which contains about 1.3M training images and 50k validation images from 1000 classes. Our model is trained for 300 epochs with Adam optimizer, whose learning rate is initialized as 0.002 and declines with a cosine decay scheme. In addition, we use the data augmentation strategies. To be fair, we use a training technique consistent with Wave-MLP, and four frameworks with close parameter numbers (T, S, M, and B). As reported in Table 4, our approach exhibits competitiveness, as described in detail in the supplementary material.

## 4 LIMITATIONS, SOCIAL IMPLICATIONS AND APPLICATION

Our model is focused on the image deblurring task, and we have tried to perform it on other image restoration tasks (such as dehazing, deraining, etc.), but it does not perform well when it comes to color restoration requirements. This may be due to the slicing scheme biasing towards the inductive bias property of the texture. In addition, our dataset does not involve sensitive information, and portrait information is solicited. In the end, we conduct a test task of object detection on the comparison method with the help of Google's API, and the experimental results show that our method helps to improve the performance of the downstream task.

Table 4: Comparison of the proposed cubic-mixer architecture with Wave-MLP model on ImageNet.

| Model | Params. | FLOPs | Top-1 acc. (%) | Model | Params | FLOPs | Top-1 acc. (%) |
|---|---|---|---|---|---|---|---|
| Wave-MLP-T | 17M | 2.4G | **80.6** | Cubic-Mixer-T | 16.5M | 2.2G | 80.5 |
| Wave-MLP-S | 30M | 4.5G | 82.6 | Cubic-Mixer-S | 31M | 4.4G | **82.7** |
| Wave-MLP-M | 44M | 7.9G | 83.4 | Cubic-Mixer-M | 40M | 7.6G | **83.5** |
| Wave-MLP-B | 63M | 10.2G | **83.6** | Cubic-Mixer-B | 59M | 9.9G | **83.6** |

## 5 RELATED WORK

**Single image deblurring in the spatial domain.** Many assumptions and priors for image deblurring have been developed including gradient priors [Chen et al., 2019, McCloskey and Langer, 2009, Perrone and Favaro, 2014], sparse representation priors [Dong et al., 2011, Krishnan et al., 2011, Xu et al., 2013], $l_0$-norm regularizers [Li et al., 2018, Xu et al., 2013], patch priors [Michaeli and Irani, 2014, Sun et al., 2013]. However, these prior-based methods are not always applicable in dynamic scenes that contain depth variations and moving objects.

Recently, due to the success of deep learning in computer vision, many CNN-based approaches have also been proposed for image deblurring [Chen et al., 2022, Gao et al., 2019, Kim et al., 2017, Kupyn et al., 2018, 2019, Suin et al., 2020, Tao et al., 2018, Zamir et al., 2021, Zhang et al., 2019a, 2018]. In addition to CNNs, Transformer-based approaches [Chen et al., 2021b, Liang et al., 2021, Tu et al., 2022, Wang et al., 2021b, Zamir et al., 2022] are also used for image deblurring. However, these methods pay attention only to the spatial domain and ignore the frequency domain information in image deblurring. In addition, all these spatial domain based deblurring methods are computationally expensive.

**Single image deblurring in the frequency domain.** There are also some methods achieve image deblurring in the frequency domain. Wiener deconvolution is a commonly used non-blind linear image recovery algorithm that performs deblurring by converting spatial domain to frequency domain [Levin et al., 2009]. In addition, several CNN-based deep network methods are proposed to act on the image frequency domain by FFT. Delbracio et al. [Delbracio and Sapiro, 2015a] proposed a Fourier aggregation method based on [Delbracio and Sapiro, 2015b] to recover a clear image in videos with multiple adjacent frames. Chakrabarti [Chakrabarti, 2016] used a CNN to learn an affine matrix in the frequency domain and then multiplied the affine matrix with the frequency domain features to recover a clear image by inverse Fourier transform (IFT). These methods have difficulty in establishing long dependencies on the Fourier coefficients due to the limited capacity of the model.

**MLP on the visual task.** Recently, there are many attempts to explore the benefits of MLP in computer vision tasks including image classification [Chen et al., 2020, Dosovitskiy et al., 2021, Kolesnikov et al., 2020, Tolstikhin et al., 2021], object detection [Zhu et al., 2020], recognition [Zhao et al., 2020], and low-level image tasks [Chen et al., 2021b, Liang et al., 2021, Tu et al., 2022, Wang et al., 2021b, Wu et al., 2020, Zamir et al., 2022]. However, these methods usually need a fine-grained CNN stem allowing the subsequent model to build long-range dependencies, which can easily cause visible streaks in the enhanced image. In this paper, we explore a novel MLP-based image deblurring approach without CNN stem to establish long-range dependencies on the image frequency domain.

**UHD image enhancement.** Some approaches [Gharbi et al., 2017, He et al., 2020, Wang et al., 2019, 2021a, Xia et al., 2020, Yuan et al., 2021, Zeng et al., 2020, Zhang and Tao, 2020] have been proposed to reconstruct high-resolution images in real-time. The bilateral filter/grid has attracted long-term attention in its acceleration [Barron and Poole, 2016, Chen et al., 2016, 2017, Zheng et al., 2021], which is an edge-aware manipulation of images in the bilateral space [Barron et al., 2015, Wang et al., 2019, Xia et al., 2020]. In this paper, we regress a full-resolution affine transformation tensor directly from the tail of the network.

**Multi-scale fusion.** Recently multiscale image fusion schemes [Chen et al., 2021a, Ke et al., 2021, Li et al., 2021, Zhang et al., 2021] are still widely adopted due to its thorough consideration of the texture and color of the image on different perceptual fields. In contrast, the multiscale network is used to recover a tensor with attention characteristics instead of recovering an image directly.

## 6 DISCUSSION AND CONCLUSION

Executing an image by multi-scale cubic-mixer can be regarded as learning one dimension of the image information with attention characteristics, and its efficiency advantage comes from the computational resources applied on low density images. In this paper, we propose a multi-scale cubic-mixer for arbitrary size image deblurring. Our algorithm learns the mapping relationship of real and imaginary components between blurry input and sharp output using multi-scale cubic-mixer. Local feature extraction, slicing strategie and multi-scale scheme help us to improve the deblurring effect. Quantitative and qualitative results show that the proposed algorithm performs favorably against the

state-of-the-art deblurring methods in terms of accuracy and inference speed, and can generate a pleasing-visually image on real-world UHD images in real time.

## References


Jonathan T. Barron and Ben Poole. The fast bilateral solver. In *ECCV*, 2016.

Jonathan T. Barron, Andrew Adams, YiChang Shih, and Carlos Hernández. Fast bilateral-space stereo for synthetic defocus. In *CVPR*, 2015.

Ayan Chakrabarti. A neural approach to blind motion deblurring. In *ECCV*, 2016.

Chun-Fu Richard Chen, Quanfu Fan, and Rameswar Panda. Crossvit: Cross-attention multi-scale vision transformer for image classification. In *CVPR*, 2021a.

Hanting Chen, Yunhe Wang, Tianyu Guo, Chang Xu, Yiping Deng, Zhenhua Liu, Siwei Ma, Chunjing Xu, Chao Xu, and Wen Gao. Pre-trained image processing transformer. In *CVPR*, 2021b.

Jiawen Chen, Andrew Adams, Neal Wadhwa, and Samuel W. Hasinoff. Bilateral guided upsampling. *ACM TOG*, 35 (6):203:1–203:8, 2016.

Liang Chen, Faming Fang, Tingting Wang, and Guixu Zhang. Blind image deblurring with local maximum gradient prior. In *CVPR*, 2019.

Liangyu Chen, Xiaojie Chu, Xiangyu Zhang, and Jian Sun. Simple baselines for image restoration. *arXiv preprint arXiv:2204.04676*, 2022.

Mark Chen, Alec Radford, Rewon Child, Jeffrey Wu, Heewoo Jun, David Luan, and Ilya Sutskever. Generative pretraining from pixels. In *ICML*, 2020.

Qifeng Chen, Jia Xu, and Vladlen Koltun. Fast image processing with fully-convolutional networks. In *ICCV*, 2017.

Mauricio Delbracio and Guillermo Sapiro. Hand-held video deblurring via efficient fourier aggregation. *IEEE Trans. Computational Imaging*, 1(4):270–283, 2015a.

Mauricio Delbracio and Guillermo Sapiro. Burst deblurring: Removing camera shake through fourier burst accumulation. In *CVPR*, 2015b.

Senyou Deng, Wenqi Ren, Yanyang Yan, Tao Wang, Fenglong Song, and Xiaochun Cao. Multi-scale separable network for ultra-high-definition video deblurring. In *ICCV*, 2021.

Weisheng Dong, Lei Zhang, Guangming Shi, and Xiaolin Wu. Image deblurring and super-resolution by adaptive sparse domain selection and adaptive regularization. *IEEE TIP*, 20(7):1838–1857, 2011.

Alexey Dosovitskiy, Lucas Beyer, Alexander Kolesnikov, Dirk Weissenborn, Xiaohua Zhai, Thomas Unterthiner, Mostafa Dehghani, Matthias Minderer, Georg Heigold, Sylvain Gelly, Jakob Uszkoreit, and Neil Houlsby. An image is worth 16x16 words: Transformers for image recognition at scale. In *ICLR*, 2021.

Hongyun Gao, Xin Tao, Xiaoyong Shen, and Jiaya Jia. Dynamic scene deblurring with parameter selective sharing and nested skip connections. In *CVPR*, 2019.

Michaël Gharbi, Jiawen Chen, Jonathan T. Barron, Samuel W. Hasinoff, and Frédo Durand. Deep bilateral learning for real-time image enhancement. *ACM TOG*, 36(4):118:1–118:12, 2017.

D. C. Ghiglia and MD Pritt. *Two-Dimensional Phase Unwrapping: Theory, Algorithms, and Software*. Two-Dimensional Phase Unwrapping: Theory, Algorithms, and Software, 1998.

Dong Gong, Jie Yang, Lingqiao Liu, Yanning Zhang, Ian D. Reid, Chunhua Shen, Anton van den Hengel, and Qinfeng Shi. From motion blur to motion flow: A deep learning solution for removing heterogeneous motion blur. In *CVPR*, 2017.

Bin He, Ce Wang, Boxin Shi, and Ling-Yu Duan. Fhde$^2$net: Full high definition demoireing network. In *ECCV*, 2020.

Rim Jaesung, Lee Haeyun, Won Jucheol, and Cho Sunghyun. Real-world blur dataset for learning and benchmarking deblurring algorithms. In *ECCV*, 2020.

Justin Johnson, Alexandre Alahi, and Fei-Fei Li. Perceptual losses for real-time style transfer and super-resolution. In *ECCV*, 2016.

Adam Kaufman and Raanan Fattal. Deblurring using analysis-synthesis networks pair. In *CVPR*, 2020.

Junjie Ke, Qifei Wang, Yilin Wang, Peyman Milanfar, and Feng Yang. Musiq: Multi-scale image quality transformer. In *ICCV*, 2021.

Tae Hyun Kim, Kyoung Mu Lee, Bernhard Schölkopf, and Michael Hirsch. Online video deblurring via dynamic temporal blending network. In *ICCV*, 2017.

Alexander Kolesnikov, Lucas Beyer, Xiaohua Zhai, Joan Puigcerver, Jessica Yung, Sylvain Gelly, and Neil Houlsby. Big transfer (bit): General visual representation learning. In *ECCV*, 2020.

Dilip Krishnan, Terence Tay, and Rob Fergus. Blind deconvolution using a normalized sparsity measure. In *CVPR*, 2011.

Orest Kupyn, Volodymyr Budzan, Mykola Mykhailych, Dmytro Mishkin, and Jiri Matas. Deblurgan: Blind motion deblurring using conditional adversarial networks. In *CVPR*, 2018.

Orest Kupyn, Tetiana Martyniuk, Junru Wu, and Zhangyang Wang. Deblurgan-v2: Deblurring (orders-of-magnitude) faster and better. In *ICCV*, 2019.

Junyong Lee, Hyeongseok Son, Jaesung Rim, Sunghyun Cho, and Seungyong Lee. Iterative filter adaptive network for single image defocus deblurring. In *CVPR*, 2021.

Anat Levin, Yair Weiss, Frédo Durand, and William T. Freeman. Understanding and evaluating blind deconvolution algorithms. In *CVPR*, 2009.

Guofa Li, Yongjie Lin, and Xingda Qu. An infrared and visible image fusion method based on multi-scale transformation and norm optimization. *Information Fusion*, 71:109–129, 2021.

Lerenhan Li, Jinshan Pan, Wei-Sheng Lai, Changxin Gao, Nong Sang, and Ming-Hsuan Yang. Learning a discriminative prior for blind image deblurring. In *CVPR*, 2018.

Jingyun Liang, Jiezhang Cao, Guolei Sun, Kai Zhang, Luc Van Gool, and Radu Timofte. SwinIR: Image restoration using swin transformer. In *CVPR*, 2021.

Scott McCloskey and Michael S. Langer. Planar orientation from blur gradients in a single image. In *CVPR*, 2009.

Tomer Michaeli and Michal Irani. Blind deblurring using internal patch recurrence. In *ECCV*, 2014.

Seungjun Nah, Tae Hyun Kim, and Kyoung Mu Lee. Deep multi-scale convolutional neural network for dynamic scene deblurring. In *CVPR*, 2017.

Seungjun Nah, Sungyong Baik, Seokil Hong, Gyeongsik Moon, Sanghyun Son, Radu Timofte, and Kyoung Mu Lee. NTIRE 2019 challenge on video deblurring and super-resolution: Dataset and study. In *CVPRW*, 2019.

Simon Niklaus, Long Mai, and Feng Liu. Video frame interpolation via adaptive convolution. In *CVPR*, 2017.

Daniele Perrone and Paolo Favaro. Total variation blind deconvolution: The devil is in the details. In *CVPR*, 2014.

Fengqing Qin, Chaorong Li, Lilan Cao, Lihong Zhu, Xuyan Zou, Xiaomei Li, Tianqi Zhang, and Yilan Xue. Blind image restoration with defocus blur by estimating point spread function in frequency domain. In *ICAIP*, 2021.

Karen Simonyan and Andrew Zisserman. Very deep convolutional networks for large-scale image recognition. In *ICLR*, 2015.

Yao Sui, Onur Afacan, Ali Gholipour, and Simon K Warfield. MRI super-resolution through generative degradation learning. In *MICCAI*, 2021.

Maitreya Suin, Kuldeep Purohit, and A. N. Rajagopalan. Spatially-attentive patch-hierarchical network for adaptive motion deblurring. In *CVPR*, 2020.

Libin Sun, Sunghyun Cho, Jue Wang, and James Hays. Edge-based blur kernel estimation using patch priors. In *ICCP*, 2013.

Yehui Tang, Kai Han, Jianyuan Guo, Chang Xu, Yanxi Li, Chao Xu, and Yunhe Wang. An image patch is a wave: Phase-aware vision MLP. In *CVPR*, 2022.

Xin Tao, Hongyun Gao, Xiaoyong Shen, Jue Wang, and Jiaya Jia. Scale-recurrent network for deep image deblurring. In *CVPR*, 2018.

Ilya Tolstikhin, Neil Houlsby, Alexander Kolesnikov, Lucas Beyer, Xiaohua Zhai, Thomas Unterthiner, Jessica Yung, Daniel Keysers, Jakob Uszkoreit, Mario Lucic, and Alexey Dosovitskiy. MLP-mixer: An all-MLP architecture for vision. *CoRR*, 2021.

Zhengzhong Tu, Hossein Talebi, Han Zhang, Feng Yang, Peyman Milanfar, Alan Bovik, and Yinxiao Li. Maxim: Multi-axis mlp for image processing. In *CVPR*, 2022.

Ruixing Wang, Qing Zhang, Chi-Wing Fu, Xiaoyong Shen, Wei-Shi Zheng, and Jiaya Jia. Underexposed photo enhancement using deep illumination estimation. In *CVPR*, 2019.

Tao Wang, Yong Li, Jingyang Peng, Yipeng Ma, Xian Wang, Fenglong Song, and Youliang Yan. Real-time image enhancer via learnable spatial-aware 3D lookup tables. In *ICCV*, 2021a.

Zhendong Wang, Xiaodong Cun, Jianmin Bao, and Jianzhuang Liu. Uformer: A general U-shaped transformer for image restoration. *arXiv preprint arXiv:2106.03106*, 2021b.

Junru Wu, Xiang Yu, Ding Liu, Manmohan Chandraker, and Zhangyang Wang. DAVID: Dual-attentional video deblurring. In *WACV*, 2020.

Xide Xia, Meng Zhang, Tianfan Xue, Zheng Sun, Hui Fang, Brian Kulis, and Jiawen Chen. Joint bilateral learning for real-time universal photorealistic style transfer. In *ECCV*, 2020.

dMao Xintian, Liu Yiming, Wei Shen, Li Qingli, and Yan Wang. Deep residual fourier transformation for single image deblurring. In *arXiv:2111.11745*, 2021.

Li Xu, Shicheng Zheng, and Jiaya Jia. Unnatural L0 sparse representation for natural image deblurring. In *CVPR*, 2013.

Dan Yang and Mehmet Yamac. Motion aware double attention network for dynamic scene deblurring. In *2022 IEEE/CVF Conference on Computer Vision and Pattern Recognition Workshops (CVPRW)*, pages 1112–1122, 2022.

Yuhui Yuan, Rao Fu, Lang Huang, Weihong Lin, Chao Zhang, Xilin Chen, and Jingdong Wang. HRFormer: High-resolution transformer for dense prediction. In *NeurIPS*, 2021.

Syed Waqas Zamir, Aditya Arora, Salman Khan, Munawar Hayat, Fahad Shahbaz Khan, Ming-Hsuan Yang, and Ling Shao. Multi-stage progressive image restoration. In *CVPR*, 2021.

Syed Waqas Zamir, Aditya Arora, Salman Khan, Munawar Hayat, Fahad Shahbaz Khan, and Ming-Hsuan Yang. Restormer: Efficient transformer for high-resolution image restoration. In *CVPR*, 2022.

Hui Zeng, Jianrui Cai, Lida Li, Zisheng Cao, and Lei Zhang. Learning image-adaptive 3D lookup tables for high performance photo enhancement in real-time. *IEEE TPAMI*, abs/2009.14468, 2020.

Hongguang Zhang, Yuchao Dai, Hongdong Li, and Piotr Koniusz. Deep stacked hierarchical multi-patch network for image deblurring. In *CVPR*, 2019a.

Jiawei Zhang, Jinshan Pan, Jimmy S. J. Ren, Yibing Song, Linchao Bao, Rynson W. H. Lau, and Ming-Hsuan Yang. Dynamic scene deblurring using spatially variant recurrent neural networks. In *CVPR*, 2018.

Jing Zhang and Dacheng Tao. Famed-Net: A fast and accurate multi-scale end-to-end dehazing network. *IEEE TIP*, 29:72–84, 2020.

Kaihao Zhang, Wenhan Luo, Yiran Zhong, Lin Ma, Wei Liu, and Hongdong Li. Adversarial spatio-temporal learning for video deblurring. *IEEE Transactions on Image Processing*, 28(1):291–301, 2019b.

Pengchuan Zhang, Xiyang Dai, Jianwei Yang, Bin Xiao, Lu Yuan, Lei Zhang, and Jianfeng Gao. Multi-scale vision longformer: A new vision transformer for high-resolution image encoding. In *CVPR*, 2021.

Hengshuang Zhao, Jiaya Jia, and Vladlen Koltun. Exploring self-attention for image recognition. In *CVPR*, 2020.

Zhuoran Zheng, Wenqi Ren, Xiaochun Cao, Tao Wang, and Xiuyi Jia. Ultra-high-definition image HDR reconstruction via collaborative bilateral learning. In *ICCV*, 2021.

Xizhou Zhu, Weijie Su, Lewei Lu, Bin Li, Xiaogang Wang, and Jifeng Dai. Deformable DETR: Deformable transformers for end-to-end object detection. *CoRR*, 2020.